

# Global emergence of regional heatwave hotspots outpaces climate model projections

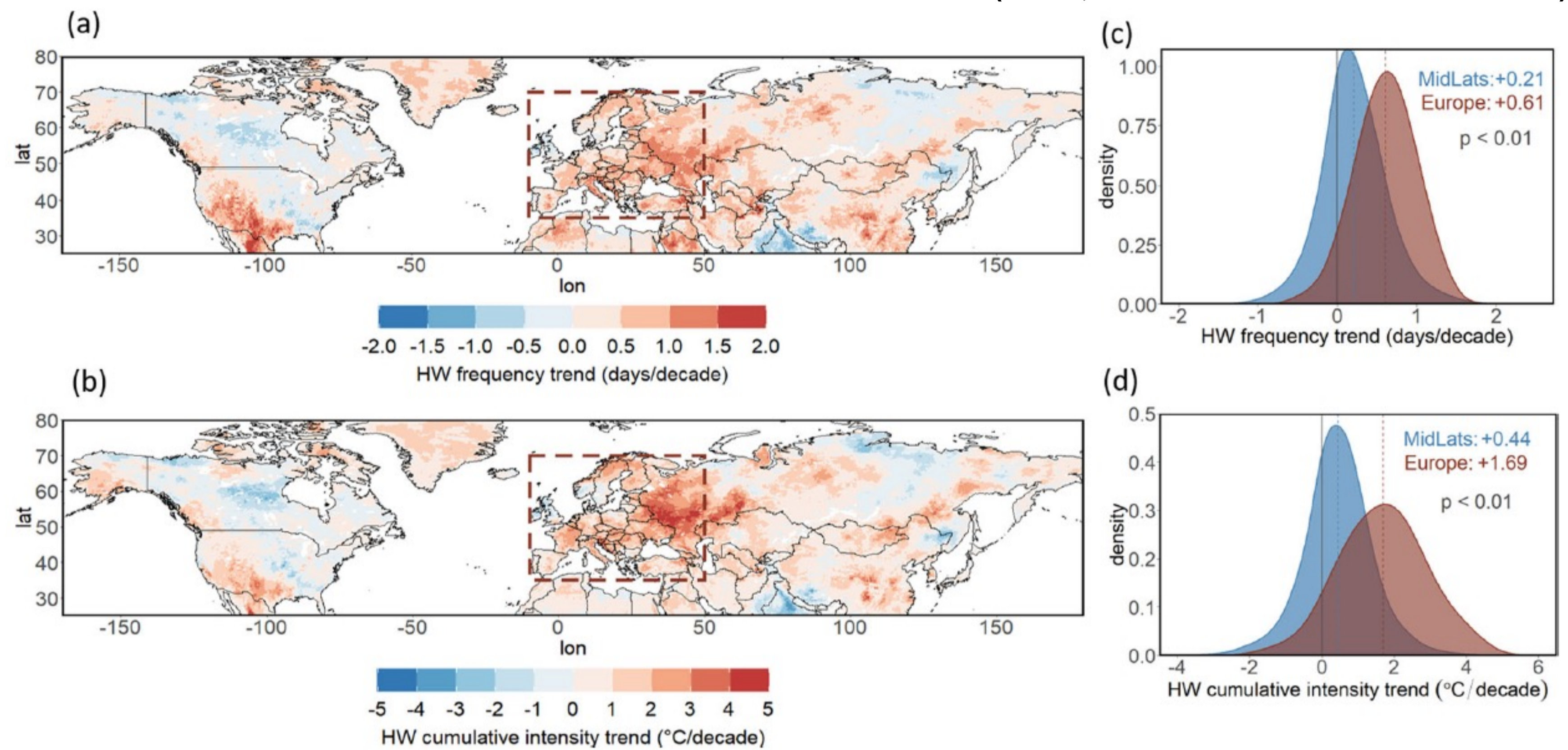
K. Kornhuber\*, S. Bartusek, R. Seager, M. Ting  
\*contact: kaik@ldeo.columbia.edu

In recent decades, hot-dry extremes have increased over Europe, at a faster rate than any other region in the mid-latitudes. Apart from thermodynamic factors, changes in large-scale dynamics have been identified as crucial factors (Rousi et al Nat. Comms. 2022), however climate models appear to underestimate the role of certain circulation patterns for extreme weather (Luo et al CWD 2020, Kornhuber et al Nat. Comms. 2023). This project will build on prior results and will investigate the projected changes of atmosphere dynamical patterns in different reanalyses and models (high-res models in CMIP6 + MPI-ESM 100-member Grand Ensemble simulations) using advanced statistical models and will quantify their importance for persistent hot-dry extremes over Central Europe. This project aims at providing crucial information on the future risks from heat-extremes over Europe and aiming at providing explanations for recent record shattering extreme weather events that might not be captured by some models.

**Fig. 1. (right) a** Decadal trends in heatwave frequency (days/decade) and **b** heatwave cumulative intensity ( $^{\circ}\text{C}/\text{decade}$ ) for July-August 1979–2020. **c** Probability density distributions of decadal trends of heatwave frequency of all land grid points for Europe (in dark red, as the region included in the dashed box of (a, b):  $35\text{--}70^{\circ}\text{N}$  and  $10\text{W--}50^{\circ}\text{E}$ ) and the midlatitudes ( $20\text{--}70^{\circ}\text{N}$ ) excluding Europe (in blue) and **d** probability density distributions of decadal trends of heatwave cumulative intensity. The mean trend for each distribution is shown with dashed vertical lines and provided on the top right of the panels. The continuous vertical lines correspond to 0 (i.e. no trend). The two distributions were compared for each case with a Kolmogorov-Smirnov test ( $p$  values shown on the center-right).

## Amplified heatwave trends over the midlatitudes and Europe

(Rousi, Kornhuber et al. Nat. Comm. 2022)



## Underestimated response to stationary Rossby Waves

(Kornhuber et al. Nat. Comm. 2023)

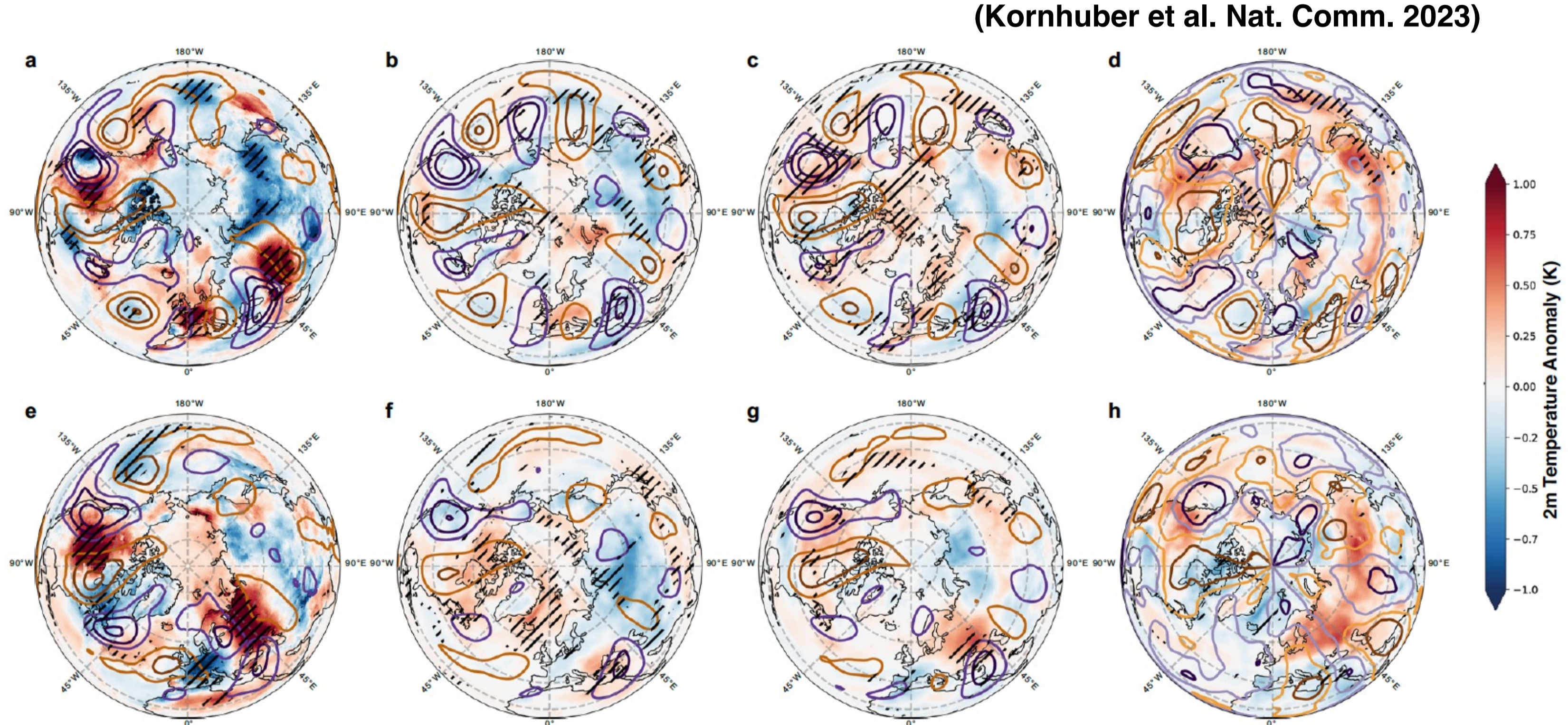


**Fig. 2** Circumglobal wave-7 and 5 patterns and associated 2m air temperature anomalies in ERA-5 reanalysis data and bias-adjusted CMIP6 models. Meridional winds in  $\text{m/s}$  (contours; purple: southerly, orange: northerly winds, in (a–c, e–g) contours start at an absolute value of  $3\text{m/s}$  and increase/decrease by 3 respectively, in (d, h) contours start an absolute value of  $0.5$  and increase/decrease by steps of one) and near surface temperature anomalies filled contours during (a–c) wave-7 and (e–g) wave-5 events relative to the respective climatology in the northern hemisphere summer (JJA) based on (a, e) ERA5 reanalysis (1960–2014), (b, f) historical (1960–2014) and (c, g) future (SSP5-8.5, 2045–2099) bias-adjusted output from CMIP6 simulations (four models). **d, h** Difference in meridional winds and temperature response during wave events comparing historical and future patterns in four bias-adjusted CMIP6 models (for twelve non adjusted models see Fig. S6). Hatching shows statistical significance on a 95% confidence level (a, d, e, h) or 100% model agreement in sign (4 out of 4 models, b, c, f, g). While the phase positions and intensity of the wave patterns (line contour) are well represented in the models their surface imprint are considerably underestimated in historical simulations. Changes in the temperature response are identified over North America, Eurasia and East Asia (d, h)

## North-Western Pacific Heatwave 2021: Non-linear interaction of common Drivers

(Bartusek, Kornhuber, Teng, Nature Clim. Ch. 2022)

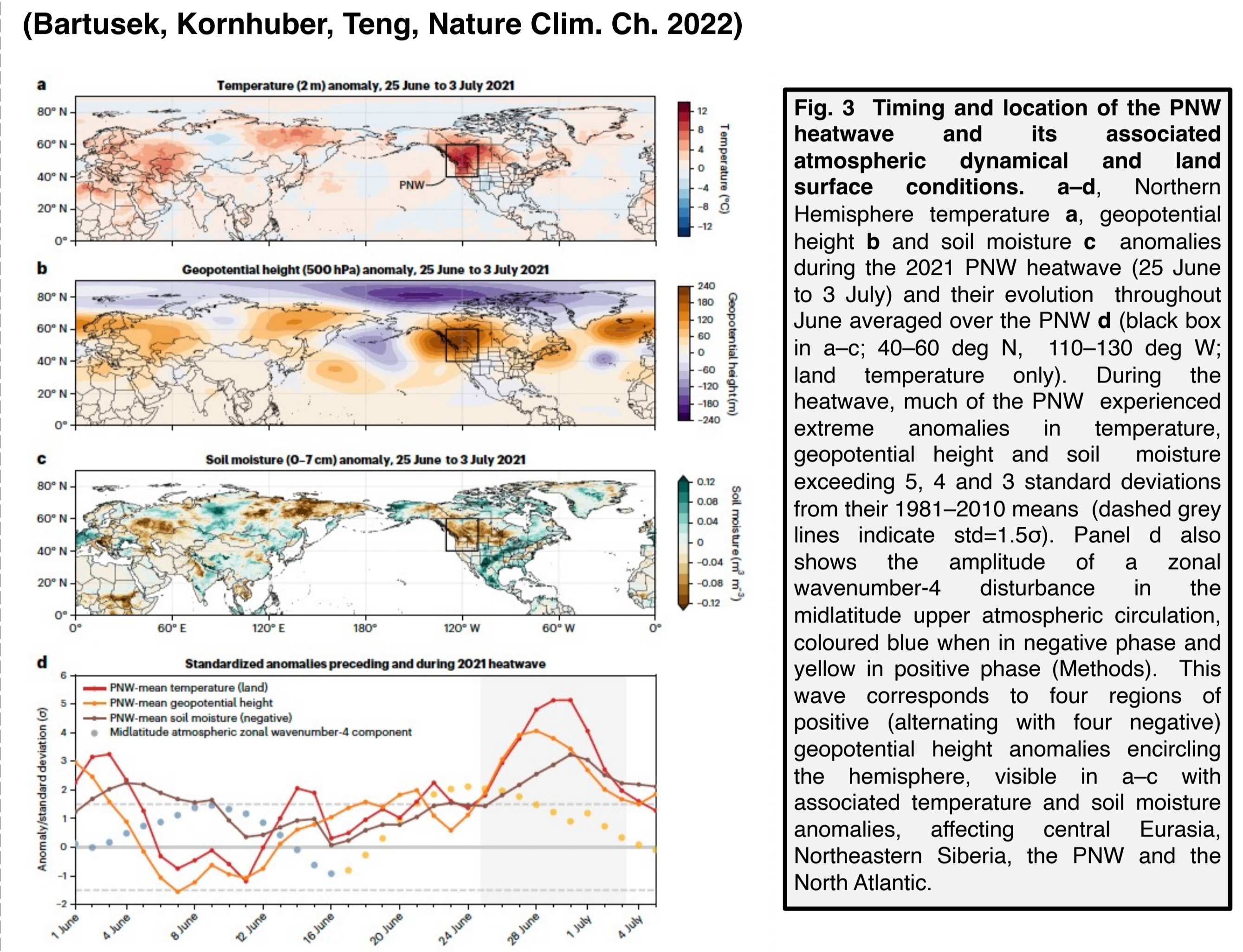


**Fig. 3** Timing and location of the PNW heatwave and its associated atmospheric dynamical and land surface conditions. **a–d**, Northern Hemisphere temperature **a**, geopotential height **b** and soil moisture **c** anomalies during the 2021 PNW heatwave (25 June to 3 July) and their evolution throughout June averaged over the PNW **d** (black box in a–c;  $40\text{--}60^{\circ}\text{N}$ ,  $110\text{--}130^{\circ}\text{W}$ ; land temperature only). During the heatwave, much of the PNW experienced extreme anomalies in temperature, geopotential height and soil moisture exceeding 5, 4 and 3 standard deviations from their 1981–2010 means (dashed grey lines indicate  $\text{std}=1.5\sigma$ ). Panel **d** also shows the amplitude of a zonal wavenumber-4 disturbance in the midlatitude upper atmospheric circulation, coloured blue when in negative phase and yellow in positive phase (Methods). This wave corresponds to four regions of positive (alternating with four negative) geopotential height anomalies encircling the hemisphere, visible in a–c with associated temperature and soil moisture anomalies, affecting central Eurasia, Northeastern Siberia, the PNW and the North Atlantic.

## Global emergence of regional heatwave hotspots outpaces climate model projections

(Kornhuber et al. (in review))

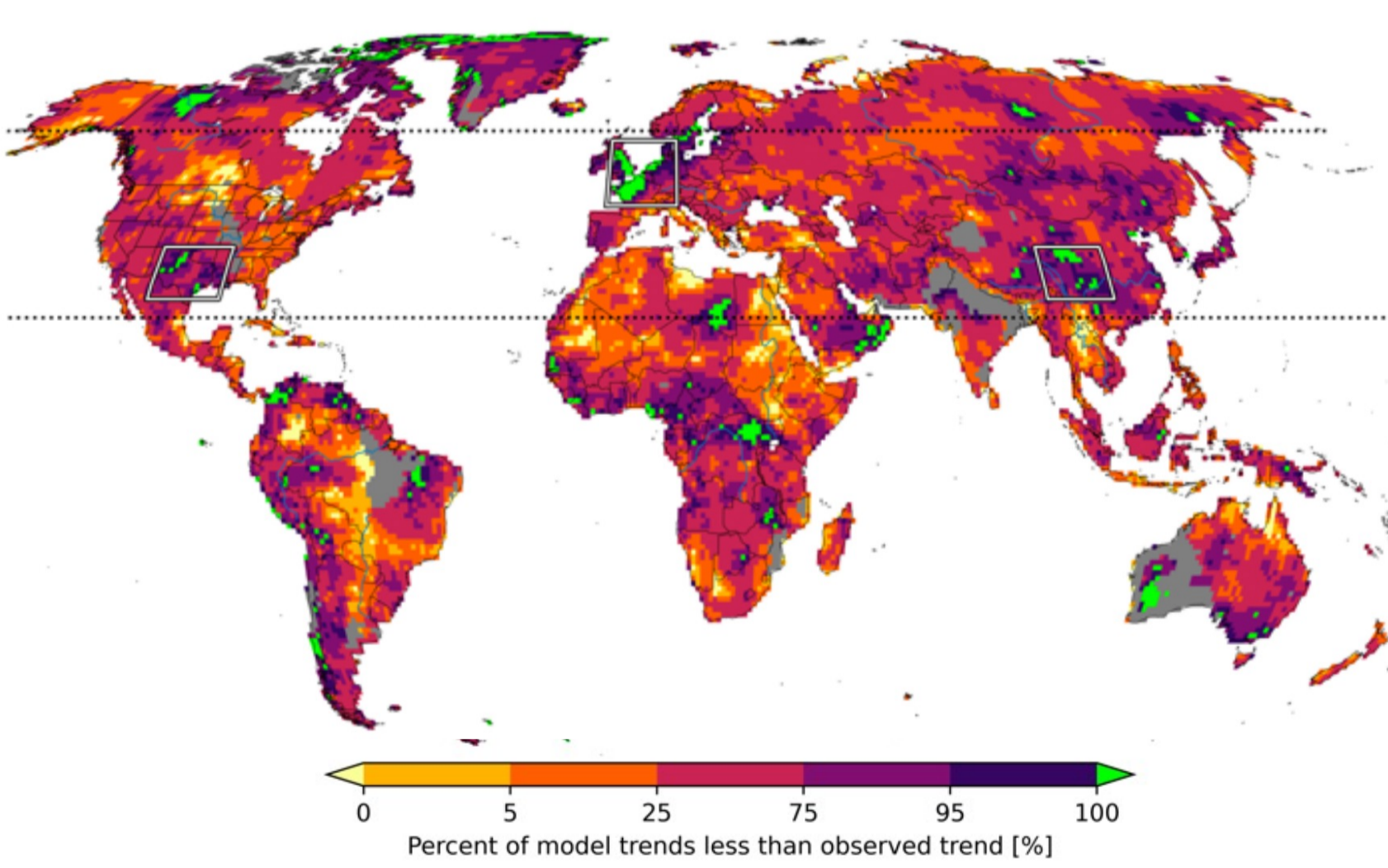


**Fig. 5 (top)** Comparison of observed trends with the range of 49 model simulations of various architectures. Observed trends are outside of the modelled range in several regions globally (light green). We estimating the changes in the differences of the hottest day (annual maximum of daily maximum temperature ( $T_x$ )) with the average of the hottest quarter of days (annual 87.5th percentile of  $T_x$  as the average of the upper quartile provided by the 75th and 100th percentile) of the annual maximum temperature at each grid point for years 1950–2022, highlights a warming of the most extreme events exceeding the underlying summer-average warming (i.e. a widening of the upper tail of the temperature distribution) in various regions globally - including North America, Europe, China (see Fig. 6).

**Fig. 6 (below)** Distributions of modelled changes in the 100th percentile compared to the 87.5th percentile in different model architectures compared to the observations, displayed as box-and whisker-plots. Boxes display 25th and 75th percentile while the median is shown as a horizontal black line. The whiskers denote the 5th and 95th percentile, while the single model values are provided as scattered 'x's. The first boxplots show the coupled and SST forced HighResMIP project model runs. The third boxplot displays regional trends from a 10-member ensemble of CAM6 forced by ERSSTv5 historical SSTs, covering 1950–2021. The fourth boxplot shows the same from a 25-member ensemble of ECHAM5 forced by ERSSTv5 covering 1950–2020, and the fifth from a 25-member ensemble of ECHAM5 forced by Hurrell SSTs covering 1950–2020. Note that the 3<sup>rd</sup>–6<sup>th</sup> boxplots include ensembles that do not cover the entire time-period 1950–2022 considered in the main analysis. The sixth boxplot aggregates all 109 model realizations.

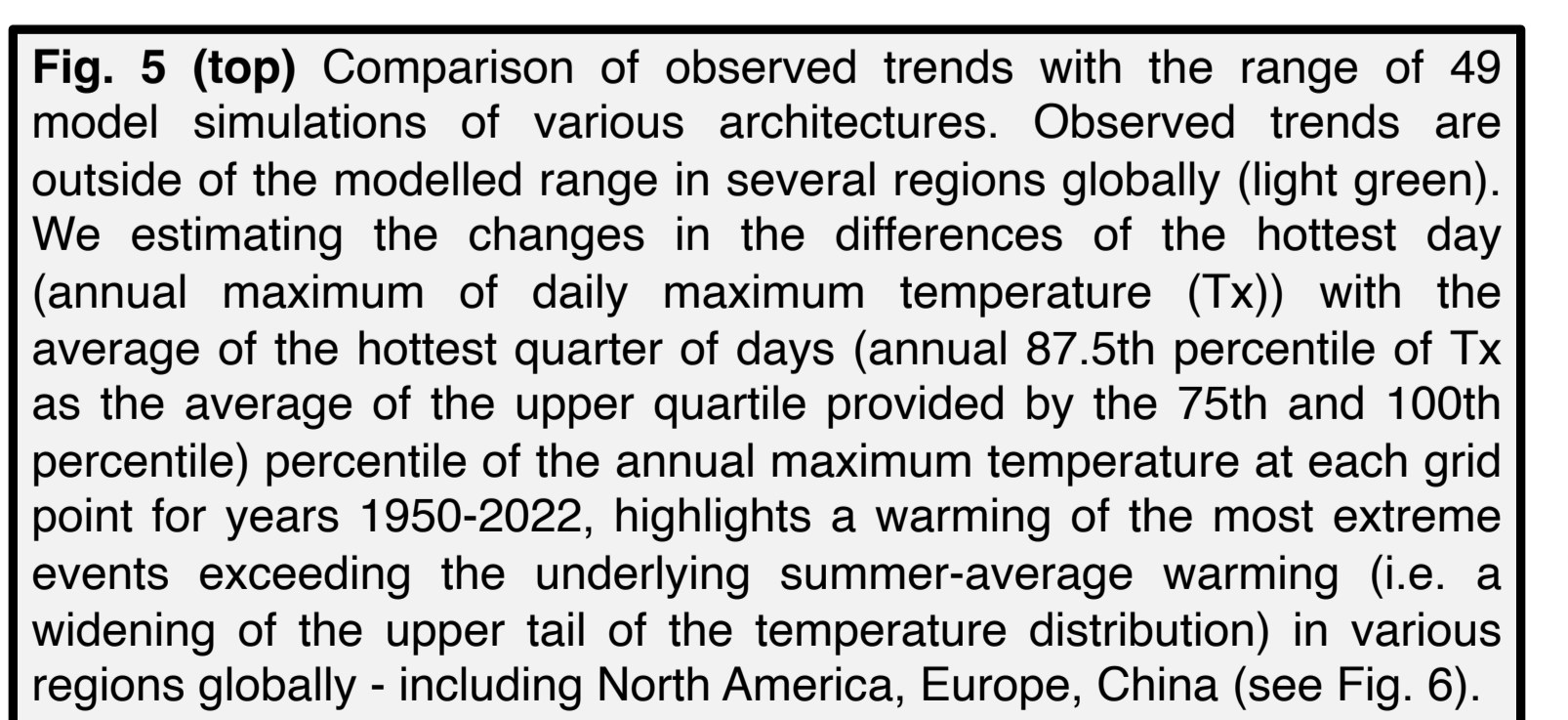


**Fig. 5 (bottom)** Regional averages of trend in temperature upper tail width for Southern North America, Northwest Europe, and Central China. Boxplots show the distribution of trends for coupled models, SST-forced models, and all models, compared to observed trends.

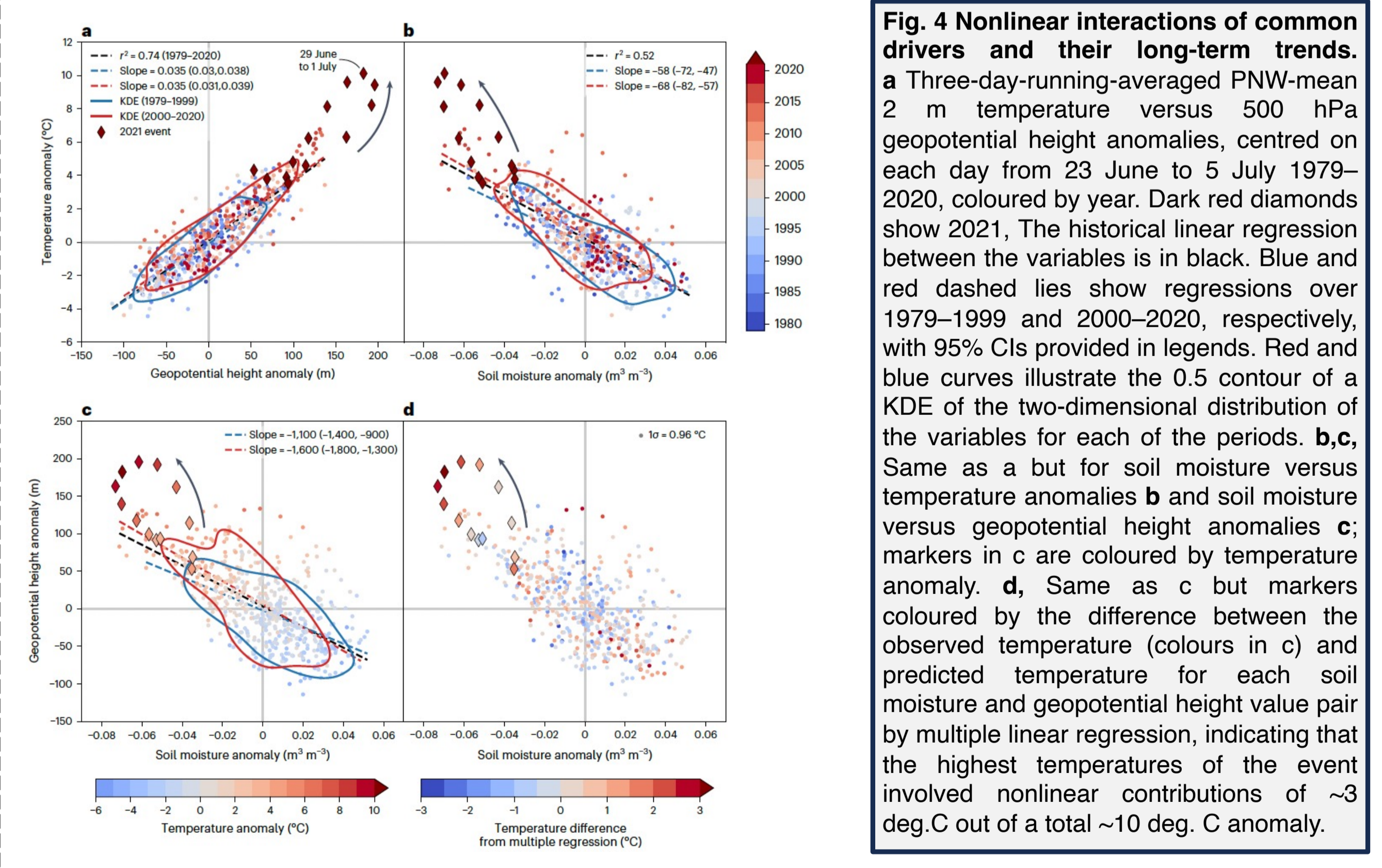


**Fig. 4** Nonlinear interactions of common drivers and their long-term trends. **a** Three-day-running-averaged PNW-mean 2 m temperature versus 500 hPa geopotential height anomalies, centred on each day from 23 June to 5 July 1979–2020, coloured by year. Dark red diamonds show 2021. The historical linear regression between the variables is in black. Blue and red dashed lines show regressions over 1979–1999 and 2000–2020, respectively, with 95% CIs provided in legends. Red and blue curves illustrate the 0.5 contour of a KDE of the two-dimensional distribution of the variables for each of the periods. **b, c**, Same as **a** but for soil moisture versus temperature anomalies **b** and soil moisture versus geopotential height anomalies **c**; markers in **c** are coloured by temperature anomaly. **d**, Same as **c** but markers coloured by the difference between the observed temperature (colours in **c**) and predicted temperature for each soil moisture and geopotential height value pair by multiple linear regression, indicating that the highest temperatures of the event involved nonlinear contributions of  $\sim 3$  deg.C out of a total  $\sim 10$  deg. C anomaly.